View metadata, citation and similar papers at core.ac.uk

brought to you by CORE

provided by Crossref

Article

Chinese Science Bulletin

Optoelectronics

October 2012 Vol.57 No.30: 3937–3942
doi: 10.1007/s11434-012-5389-3

The effect of multi-quantum barrier structure on light-emitting diodes performance by a non-isothermal model

WANG TianHu[1], XU JinLiang[2*] & WANG XiaoDong[2*]

[1] *Beijing Key Laboratory of New and Renewable Energy, North China Electric Power University, Beijing 102206, China;*
[2] *Beijing Key Laboratory of Multiphase Flow and Heat Transfer for Low Grade Energy, North China Electric Power University, Beijing 102206, China*

Received April 26, 2012; accepted June 4, 2012

A multi-quantum barrier structure is employed as the electron blocking layer of light-emitting diodes to enhance their performance. Using the non-isothermal multi-physics-field coupling model, the internal quantum efficiency, internal heat source characteristics, spectrum characteristics, and photoelectric conversion efficiency of light-emitting diodes are analyzed systematically. The simulation results show that: introducing multi-quantum barrier electron blocking layer structure significantly increases the internal quantum efficiency and photoelectric conversion efficiency of light-emitting diodes and the intensity of spectrum, and strongly ensures the thermal and light output stability of light-emitting diodes. These results are attributed to the modified energy band diagrams of the electron blocking layer which are responsible for the decreased electron leakage and enhanced carrier concentration in the active region.

light-emitting diodes, internal quantum efficiency, multi-quantum barrier, spectrum intensity, electron leakage

Citation: Wang T H, Xu J L, Wang X D. The effect of multi-quantum barrier structure on light-emitting diodes performance by a non-isothermal model. Chin Sci Bull, 2012, 57: 3937–3942, doi: 10.1007/s11434-012-5389-3

Light-emitting diodes (LEDs) have wide commercial applications due to the low energy consumption, long lifetime and compact size. Applications include flat panel displays and lighting, traffic lights, back lighting in liquid crystal displays and white LEDs [1–4]. For high power applications, LEDs operate at high current densities, yielding remarkable efficiency droops [5]. The poor hole injection efficiency and enhanced electron current leakage in the active region may play important roles to reduce the efficiency of GaN-based LEDs. This is due to the fact that holes in GaN-based materials have relatively large effective mass to yield very low mobility [6,7].

To prevent electron overflow, a p-type $Al_xGa_{1-x}N$ layer has been inserted between the p-type GaN layer and multi-quantum wells as an electron blocking layer (EBL) [8–11]. At this stage, the p-type $Al_xGa_{1-x}N$ EBL has been widely applied in III-nitride LEDs. However, the p-type $Al_xGa_{1-x}N$ with a high Al content generally suffers from low hole concentration, which is caused by the high Mg acceptor activation energy. Besides, the p-type $Al_xGa_{1-x}N$ with a high Al content is affected by the large polarization field in $Al_xGa_{1-x}N$ EBL which reduces the effective barrier height for electrons to effectively suppress the carrier overflow [12]. Iga et al. [13] predicted that the multi-quantum barrier (MQB) can raise the "effective" barrier height in 1986 for the first time. Such effect was experimentally verified for GaInP/AlInP red laser diodes by Kishino et al. [14] in 1991. Following then, various MQB EBL structures have been proposed and applied in LED chips to overcome the shortcoming of p-type $Al_xGa_{1-x}N$ EBL. Hidaki et al. [15] reported the significantly increased external quantum efficiency with an AlGaN/AlGaN MQB EBL. Kim et al. [16] introduced an AlGaN/GaN/InGaN MQB EBL to suppress the electron overflow and enhance the hole transport to InGaN quantum wells. These investigations have confirmed that the MQB EBL is effective to improve the LED efficiency at

*Corresponding authors (email: xjl@ncepu.edu.cn; wangxd99@gmail.com)

© The Author(s) 2012. This article is published with open access at Springerlink.com

high current densities.

However, all of these R&D are performed by isothermal models, not considering the non-uniform heat conduction and dissipation within LED chips. In fact, the carrier transport and recombination process in LED chips determine the internal heat source, causing significant temperature gradients within a working LED chip. Furthermore, the carrier diffusion coefficient, mobility, transport, recombination and energy band structures are affected by local temperatures, which can not be considered by isothermal models. In [17], a non-isothermal multi-physics-field coupling model was established, and the internal non-uniform heat source distribution and temperature field of the LED chip were precisely characterized. The comparison study of the internal quantum efficiency between the non-isothermal and isothermal models was also performed, and it draws a conclusion that the isothermal model can not estimate the LED performance accurately, thus, a non-isothermal model was indeed required under large current injection conditions. In order to accurately predict chip performance under high operation current, our newly developed non-isothermal multi-physics-field coupling model will be used in this paper, the thermal-dependent spectrum characteristics, photoelectric conversion efficiency as well as internal quantum efficiency will be systematically studied by introducing a MQB EBL. Moreover, comparison was performed for LEDs with a single barrier EBL (conventional design) and MQB EBL to yield a better understanding of the enhancement mechanism by MQB EBL through a perspective of thermal effect.

1 LED structures and simulation parameters

Two LED structures were used in this paper (named as samples A and B, respectively). The LED structure (see Figure 1), was prepared on a *c*-plane (0001) sapphire substrate. Before the growth of InGaN/InGaN multi-quantum wells, a 50-nm-thick un-doped GaN buffer layer was deposited and then a 3-μm-thick Si-doped n-type GaN layer was grown (n-doping=5×10^{18} cm^{-3}). The active region consists of five 4-nm-thick $In_{0.08}Ga_{0.92}N$ quantum wells, separated by six 10-nm-thick $In_{0.02}Ga_{0.98}N$ barriers. On top of the active region was a 20-nm-thick p-type EBL (p-doping $=5\times10^{17}$ cm^{-3}) and a 0.25-μm-thick p-type GaN cap layer (p-doping $=1\times10^{18}$ cm^{-3}). For a conventional LED, referred to as sample A here, the EBL is a single barrier p-type $Al_{0.15}Ga_{0.85}N$ EBL. The sample B uses a four-pair p-type $Al_{0.15}Ga_{0.85}N$/GaN multi-quantum barrier as the EBL. The substrate and active region have widths of 300 and 200 μm, respectively. The widths of the n-contact and p-contact are 50 and 80 μm, respectively.

Based on our previous work [17], a complete non-isothermal multi-physics-field coupling model is used here, incorporating the thermal generation and dissipation effect

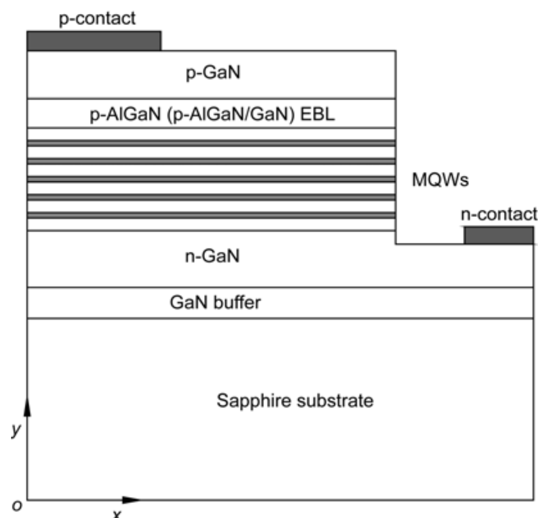

Figure 1 Schematic of LED structure.

considered by energy equation over an entire LED. The model assumes that: (1) The LED chip operates in a steady state, (2) there is no thermal contact resistance at the hetero-interface between two adjacent layers and temperature and heat flux are continuous across such internal interfaces, (3) the isothermal boundary condition is used on the bottom substrate surface with a temperature of T=313 K. Other surfaces enclosing the LED chip are adiabatic. The model includes the Poisson's equation for potential distribution, current continuity equations for transport and distribution of electrons and holes in LED structure, energy equation for temperature distribution. We solve the Poisson and Schrödinger equations for the carrier discrete energy levels and wave functions in quantum wells self-consistently. Besides, the energy band structures are calculated based on a self-consistent 6-band $k\cdot p$ method for wurtzite semiconductor [18]. Most of parameters for material properties such as GaN, AlGaN and InGaN are cited from [19]. The governing equations can be found in [17].

The total current consists of carriers that generate photons in the quantum wells (I_{rad}) and carriers that are lost due to other processes. Generally, carrier losses can occur inside or outside of quantum wells. Non-radiative recombination processes inside the quantum wells can either be defect-related Shockley-Read-Hall (SRH) recombination (I_{SRH}) or Auger recombination (I_{Auger}). Carrier recombination mechanisms outside of quantum wells are summarized as carrier leakage (I_{leak}). Thus, the total LED injection current can be written as follows:

$$I = I_{rad} + I_{SRH} + I_{Auger} + I_{leak} . \quad (1)$$

The internal quantum efficiency (IQE) can be defined as the radiative recombination inside the quantum wells divided by the total current I which can be expressed as

$$IQE = \frac{I_{rad}}{I} . \quad (2)$$

2 Results and discussion

Figure 2 shows the IQEs of samples A and B as a function of injection currents. It is found that the IQE of sample B is higher than that of sample A over the whole range of injection currents. The degree of efficiency droop is defined as (IQE_{max}–$IQE_{I=600A/m}$)/IQE_{max}. The calculation results show that the degree of efficiency droop is 22.22% and 9.37% for samples A and B, respectively. The peak value of IQE is 39% and 44%, respectively. The corresponding injection current is 201 A/m and 270 A/m, respectively. These results indicate that the LED with MQB EBL has significantly improved IQE, which is benefit for the LED operation at high injection currents.

Figure 3 shows the conduction band diagrams of samples A and B at the injection current of 600 A/m. The higher IQE of sample B than that of sample A is explained as follows. On the one hand, the AlGaN film generally suffers from lower hole concentration caused by the higher Mg acceptor activation energy, yielding the lower p-type conductivity. Because the MQB EBL structure includes p-type GaN layers, the activation energy is lower for Mg dopant in the GaN than that in the AlGaN. Thus the Mg dopant is more easily activated in the p-type AlGaN/GaN MQB EBL than that in the single barrier AlGaN EBL. Thus the effective barrier height of AlGaN/GaN MQB EBL is higher than that of the AlGaN single barrier EBL (see Figure 3). On the other hand, Based on the reflectivity ratio and transition ratio of electrons in multi-quantum barrier computed by the one-dimensional Schrödinger equation (Iga et al. [13]), the electron reflectivity is significantly increased in MQB EBL than that in single barrier EBL. Correspondingly, the effective barrier height is increased in MQB EBL. Thus the MQB EBL structure enhances the confinement of electrons. Due to the increased barrier height and reflectivity ratio of electrons, the current leakage in sample B is significantly smaller than that in sample A (see Figure 4). It is also noted that an important reason for the reduced recombination rates of electrons and holes in quantum wells is the great strain in single barrier EBL structures. But the AlGaN/GaN MQB EBL has smaller strain than the single EBL structure [20], improving the recombination rates in quantum wells.

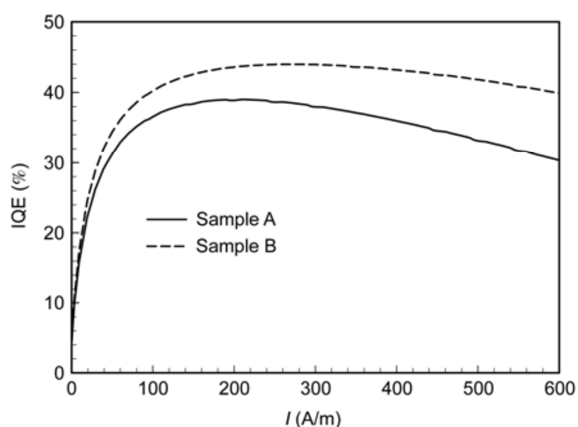

Figure 2 The IQE as a function of injection current for samples A and B.

Figures 4 and 5 further verify the above analysis. Because the MQB EBL increases the barrier height in the conduction band, enhances the electron reflectivity ratio, and decreases the strain at the interface between the last barrier and the EBL, the electron overflowing from the active region to the p-type layer is suppressed effectively, leading to the significantly smaller current leakage of sample B than that of sample A. Figure 4 shows the current leakage ratio as a function of injection currents. The current leakage ratio is defined as the current leakage which overflow from the active region to the p-type layer divided by the injection current ($\delta = I_{leak}/I$). Figure 4 indicates that δ of sample B is greatly less than that of sample A at the same injection current. δ for both structures are increased with increases in injection currents. The difference of δ between the two samples becomes larger if injection currents increase.

When the electrons overflowing to the p-type layer are diminished, the electron concentration in the active region

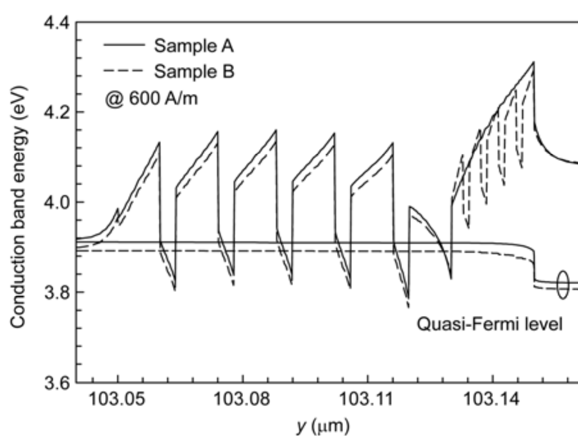

Figure 3 The conduction band diagrams for samples A and B at injection current of 600 A/m.

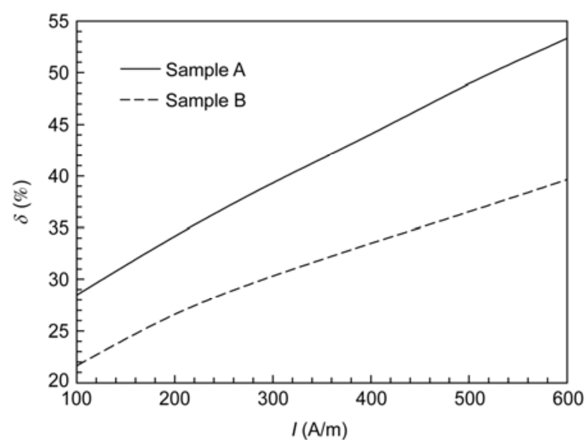

Figure 4 The current leakage ratio as a function of injection current for samples A and B.

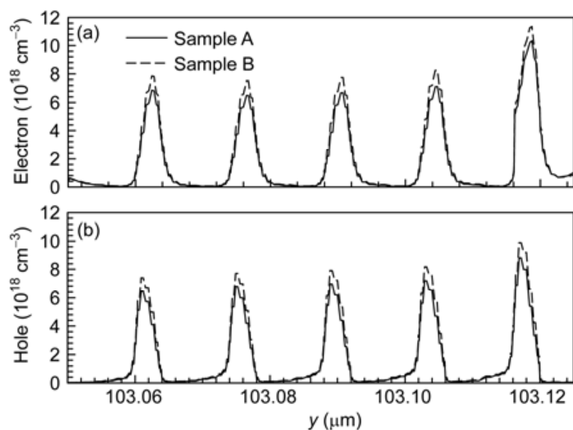

Figure 5 The carrier concentration for samples A and B at injection current of 600 A/m. (a) Electron; (b) hole.

will increase. The hole injection efficiency into the active region could be enhanced because there are fewer holes that would recombine with leaked electrons before they are injected into the active region. Therefore, carrier concentration and recombination rate in the active region are enhanced, reducing the non-radiative recombination and Joule heat effect in the p-type region. Figure 5 shows the electron and hole concentrations of the two structures at 600 A/m. In all of the quantum wells, both of electron and hole concentrations of the sample B increase. The concentrations of electrons and holes within the active region are enhanced by 13.75% and 13.46% for the sample B, respectively, when compared to those of the sample A. Due to the above mentioned advantages of the sample B, the desired radiative recombination rates within the active region of the sample B are increased (see Figure 6(a)), which in turn improves the IQE (see Figure 2).

Figure 6 shows the recombination rate for samples A and B at the injection current of 600 A/m. the recombination rate consists of radiative recombination rate, SRH recombination rate and Auger recombination rate. The light output performance is improved due to the enhanced radiative recombination rate caused by the increased carrier concentration in the active region. Simultaneously, the non-radiative recombination rate is also increased (see Figure 6(b),(c)), leading to the raised recombination heat. Figure 7 shows the internal heat source intensities versus injection currents. It is indicated that the Joule heat and recombination heat contribute the major part of the whole heat generation. The Thomson heat and Peltier heat contribute less so that they can be neglected [17]. Thus Figure 7 only plots the Joule heat, recombination heat and total heat source as a function of injection currents. Seeing from Figure 7, even though the Joule heat is decreased for sample B, the non-recombination heat is increased, causing the non-change of the total heat source intensity when the injection currents increase. It is proved that the total heat source does not change with increases in the radiative recombination rates after introducing the MQB EBL structure. This is due to the fact that the Joule heat effect becomes smaller as the decreased electron leakage. On the other hand, the radiative and non-radiative recombination rates in the active region are increased simultaneously (see eq. (1)). The combination effect of the Joule heat and recombination heat cause non-change of the total heat source intensity. Figures 8 and 9 show a comparison of epilayer temperature profiles of samples A and B at the injection current of 600 A/m. The two samples exhibit similar temperature distributions because the two samples generate almost the same heat. Thus it is concluded that the

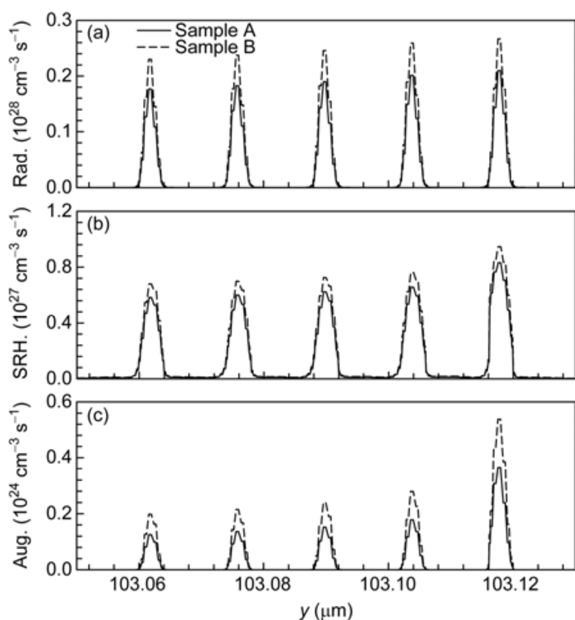

Figure 6 The recombination rate for samples A and B at injection current of 600 A/m. (a) Radiative; (b) SRH; (c) Auger.

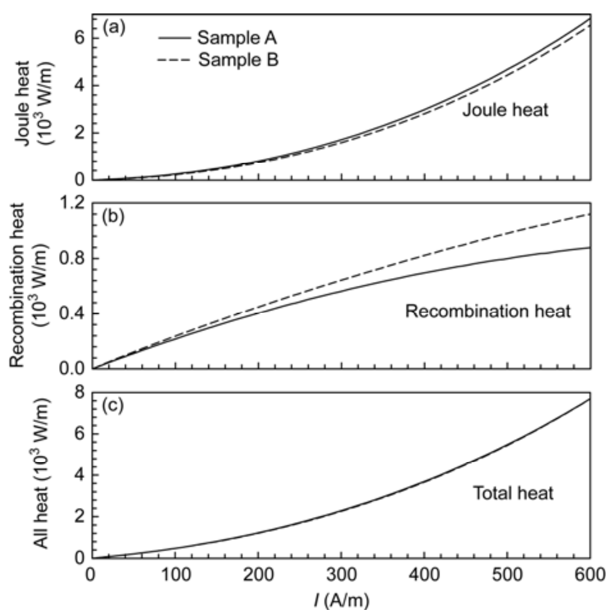

Figure 7 The internal heat source as a function of injection current for samples A and B. (a) Joule heat; (b) recombination heat; (c) total heat.

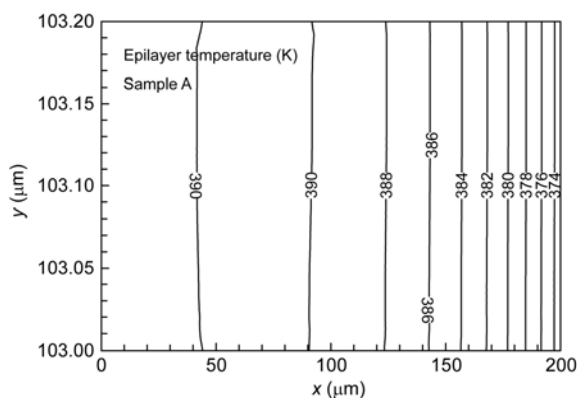

Figure 8 The epilayer temperature profile for sample A at injection current of 600 A/m.

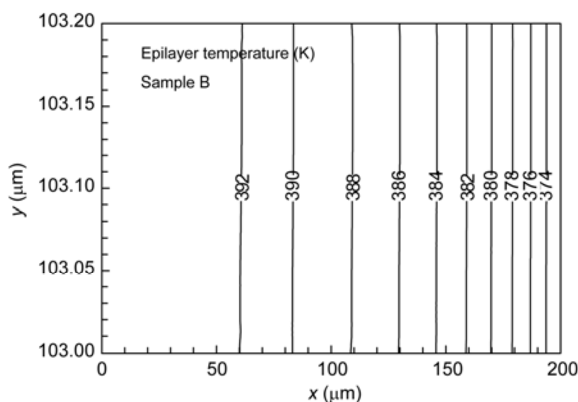

Figure 9 The epilayer temperature profile for sample B at injection current of 600 A/m.

IQE is improved but the structure temperatures are not increased by introducing the MQB EBL structure.

Figure 10 shows the light spectrum characteristics as a function of injection currents for samples A and B. It is seen from Figure 10 that the sample B holds higher spectrum intensity than the sample A at the same injection current. The intensity difference between the two samples becomes larger by increasing the injection currents. For instance, the sample B intensity is 11.7% and 28.3% higher than those of the sample A at the injection currents of 100 and 600 A/m, respectively. Besides, it is observed that the spectrum of sample B does not exhibit peak shift, compared with that of the sample A at the same injection current. Yang et al. [21] reported the noticeable red shift of the LED spectrum due to self-heating effect. But Figures 8 and 9 show the similar temperature profiles for samples A and B, leading to almost the same heat effect. Thus there is no peak shift due to the non-change of the energy band gap of the multi-quantum wells, demonstrating the light output stability of LEDs by using the MQB EBL structure.

Our non-isothermal model computations are consistent with the experimental findings by Yang et al. [21]. Two injection current modes were used in [21]. In the pulsed injection current mode (corresponding to the isothermal model), the spectrum exhibits a monotonic blue-shift over the entire current range. In the continuous wave (CW) injection current mode, a blue-shift of the emission peak is seen at small injection current, but the high injection current yields a red shift of the emission peak due to the non-isothermal effect, this result is consistent with our non-isothermal spectrum characteristics (see Figure 10) which support the red-shift emission peak under high operation current.

The photoelectric conversion efficiency η is defined as the spontaneous emission power divided by the input electric power, which is an important parameter for LED performance evaluation. Figure 11 illustrates the photoelectric conversion efficiency η for samples A and B. It is obvious that η of both samples decrease with increases in injection currents. The η of sample B is higher than that of sample A over the whole range of injection currents. The increase degree of photoelectric conversion efficiency ζ is defined as $\zeta=(\eta_B-\eta_A)/\eta_A$, where η_B is the photoelectric conversion efficiency for the sample B and η_A is for the sample A. It is

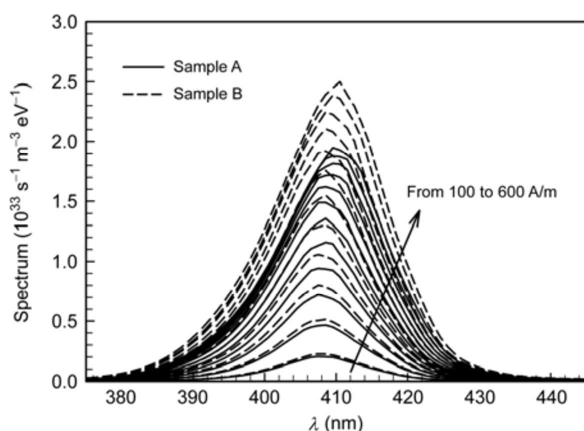

Figure 10 The spectrum characteristic as a function of injection current for samples A and B.

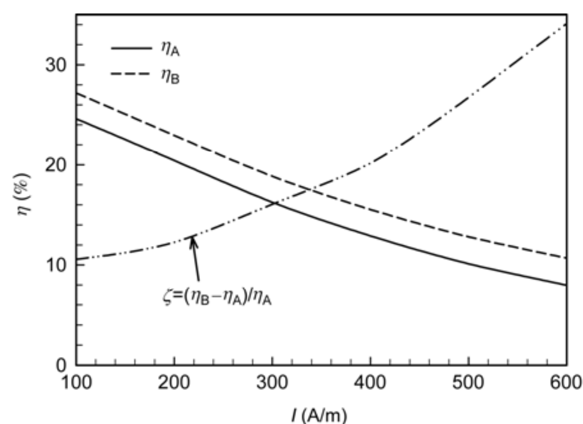

Figure 11 The photoelectric conversion efficiency as a function of injection current for samples A and B.

seen that ζ increases with increases in the injection currents, attaining the maximum value of 34.1% at the injection current of 600 A/m to show the better LED performance at high injection current by using the MQB EBL structure. This is consistent with the degree of efficiency droop shown in Figure 2 indicating much smaller degree of efficiency droop for the sample B than that for the sample A.

3 Conclusions

Based on the non-isothermal multi-physics-field coupling model, comparison study of LEDs with a single barrier EBL (conventional design) and MQB EBL (named as sample A and sample B, respectively) was performed. The internal quantum efficiency, internal heat source intensities, spectrum, and photoelectric conversion efficiency are analyzed systematically. The conclusions can be summarized as follows:

(i) Introducing a MQB EBL structure significantly increases the IQE for the sample B. The degree of efficiency droop is significantly decreased by 12.85% when compared to the sample A. The injection current corresponding to the peak value can reach up to 270 A/m.

(ii) For sample B, the total heat source intensity does not increase even with the increased radiative recombination rate after introducing the MQB EBL structure. The two samples exhibit similar temperature profiles. This increases the energy conversion efficiency from electric power to light output power and ensures the thermal stability of LED.

(iii) The sample B demonstrates higher spectrum intensity than the sample A at the same injection current. The intensity difference between the two samples becomes larger with increases in the injection currents. The spectrum for sample B does not exhibit the peak shift compared to the sample A at the same injection current, ensuring the light output stability of LEDs.

(iv) The photoelectric conversion efficiency of sample B is higher than that of sample A. The increase degree of photoelectric conversion efficiency ζ increases with the injection currents, attaining the maximum value of 34.1% at the injection current of 600 A/m. These results indicate the better performance of LEDs holding the MQB EBL structure at high injection currents.

This work was supported by the National Natural Science Foundation of China (U1034004 and 50825603), the National Basic Research Program of China (2011CB710703) and the Fundamental Research Funds for the Central University (11ZG01).

1 Shur M S. Solid-state lighting: Toward superior illumination. Proc IEEE, 2005, 93: 1691–1703
2 Krames M R, Shchekin O B, Mueller-Mach R, et al. Status and future of high-power light-emitting diodes for solid-state lighting. IEEE J Display Technol, 2007, 3: 160–175
3 Liu Q, Duan L, Zhang D Q, et al. Transparent organic light-emitting diodes based on Cs_2CO_3:Ag/Ag composite cathode. Chin Sci Bull, 2010, 55: 1479–1482
4 Zhang W W, Wu Z X, Zhang X W, et al. Dependence of the stability of organic light-emitting diodes on driving mode. Chin Sci Bull, 2011, 56: 2210–2214
5 Kim M H, Schubert M F, Dai Q, et al. Origin of efficiency droop in GaN-based light-emitting diodes. Appl Phys Lett, 2007, 91: 183507
6 David A, Grundmann M J, Kaeding J F, et al. Carrier distribution in (0001) InGaN/GaN multiple quantum well light-emitting diodes. Appl Phys Lett, 2008, 92: 053502
7 Wang C H, Chen J R, Chiu C H, et al. Temperature-dependent electroluminescence efficiency in blue InGaN-GaN light-emitting diodes with different well widths. IEEE Photon Technol Lett, 2010, 22: 236–238
8 Chitnis A, Zhang J P, Adivarahan V, et al. Improved performance of 325-nm emission AlGaN ultraviolet light-emitting Diodes. Appl Phys Lett, 2003, 82: 2565–2567
9 Tu R C, Tun C J, Pan S M, et al. Improvement of near-ultraviolet InGaN-GaN light-emitting diodes with an AlGaN electron-blocking layer grown at low temperature. IEEE Photon Technol Lett, 2003, 15: 1342–1344
10 Kim K H, Fan Z Y, Khizar M, et al. AlGaN-based ultraviolet light-emitting diodes grown on AlN epilayers. Appl Phys Lett, 2004, 85: 4777–4779
11 Hirayama H. Quaternary InAlGaN-based high-efficiency ultraviolet light-emitting diodes. J Appl Phys, 2005, 97: 091101
12 Han S H, Lee D Y, Lee S J, et al. Effect of electron blocking layer on efficiency droop in InGaN/GaN multiple quantum well light-emitting diodes. Appl Phys Lett, 2009, 94: 231123
13 Iga K, Uenohara H, Koyama F. Electon reflectance of multiquantum barrier (MQB). Electron Lett, 1986, 22: 1008–1010
14 Kishino K, Kikuchi A, Kaneko Y, et al. Enhanced carrier confinement effect by the multiquantum barrier in 660 nm GaInP/AlInP visible lasers. Appl Phys Lett, 1991, 58: 1822–1824
15 Hideki H, Yusuke T, Tetsutoshi M, et al. Marked enhancement in the efficiency of deep-ultraviolet AlGaN light-emitting diodes by using a multiquantum-barrier electron blocking layer. Appl Phys Expr, 2010, 3: 031002
16 Kim K S, Kim J H, Jung S J, et al. Stable temperature characteristics of InGaN blue light emitting diodes using AlGaN/GaN/InGaN superlattices as electron blocking layer. Appl Phys Lett, 2010, 96: 091104
17 Wang T H, Wang X D, Xu J L. The investigation of high power LED by a non-isothermal coupling model (in Chinese). J Engineer Thermophys, 2012, 33: 647–650
18 Chuang S L, Chang C S. k · p method for strained wurtzite semiconductors. Phys Rev B, 1996, 54: 2491–2504
19 Vurgaftman I, Meyer J R. Band parameters for nitrogen-containing semiconductors. J Appl Phys, 2003, 94: 3675–3696
20 Chiaria S, Furno E, Goano M, et al. Design criteria for near-ultraviolet GaN-based light-emitting diodes. IEEE Trans Electron Dev, 2010, 57: 60–70
21 Yang Y, Cao X A, Yan C H. Investigation of the nonthermal mechanism of efficiency rolloff in InGaN light-emitting diodes. IEEE Trans Electron Dev, 2008, 55: 1771–1775

Open Access This article is distributed under the terms of the Creative Commons Attribution License which permits any use, distribution, and reproduction in any medium, provided the original author(s) and source are credited.